Acoustic Analysis of Wave-guide and MEMS Microphone in Camera including Thermoviscous losses

Thesis · June 2018

DOI: 10.13140/RG.2.2.13275.05922

1 author:

Karolis Poskus
Blekinge Institute of Technology
1 PUBLICATION **0** CITATIONS

SEE PROFILE

Master of Science in Mechanical Engineering
June 2018

Acoustic Analysis of Wave-Guide and MEMS Microphone in Camera Including Thermoviscous Losses

Karolis Poskus

Faculty of Engineering, Blekinge Institute of Technology, 371 79 Karlskrona, Sweden

This thesis is submitted to the Faculty of Engineering at Blekinge Institute of Technology in partial fulfillment of the requirements for the degree of Master of Science in Mechanical Engineering. The thesis is equivalent to 20 weeks of full time studies.

The authors declare that they are the sole authors of this thesis and that they have not used any sources other than those listed in the bibliography and identified as references. They further declare that they have not submitted this thesis at any other institution to obtain a degree.

Contact Information:
Author(s):
Karolis Poskus
E-mail: kapo13@student.bth.se

University advisor:
Professor Claes Hedberg
Department of Mechanical Engineering

Faculty of Engineering
Blekinge Institute of Technology
SE–371 79 Karlskrona, Sweden

Internet : www.bth.se
Phone : +46 455 38 50 00
Fax : +46 455 38 50 57

Abstract

Today Micro Electrical Mechanical Systems (MEMS) microphones are available in a range of electronic consumer products such as smart phones, tablets, smart watches and surveillance cameras. The MEMS microphones are usually attached to a circuit board with a hole that lets sound propagate through, as well as additional wave-guides which alter the MEMS microphones original frequency response. The MEMS microphone and additional wave-guides are in the same size order as the thermal and viscous boundary layers. These are called non-ideal losses and are usually not considered when dealing with large scale acoustical systems. The only way to predict the impact of these losses is the use of Finite Element software.

The objective of the work is to model the thermoviscous losses when the waves propagate through narrow regions. The system of study is the Axis Network Camera P1367 and the study focuses on the acoustic path into the microphone. The first aim is to model the acoustic path along with the MEMS microphone to produce a frequency response that matches the measured frequency response of the different configurations for the sound-guide. A second aim is to find the configuration which produces the most desirable frequency response.

Several measurements with different configurations were made, such as varying the length and radius of the sound-guide hole. All measurements were performed in an an-echoic chamber. Thereafter, a FEM model was created of the simplified acoustic path and the different configurations that were performed in the measurement were compared with the simulated results.

The simulated frequency responses differ in terms of where the resonance frequency occurs, but the configurations of the sound-guide match the overall behavior when comparing the simulated and measured results. The most optimal configuration of the acoustical path is obtained.

The simulated model requires more work in terms of obtaining a better matching frequency response, most importantly the MEMS cavity. The real geometry of the MEMS sensor cavity did not produce the same frequency response as the one in the data sheet for the specific microphone used for this study, thus a fictive cavity was introduced to produce the desired frequency response. The model did succeed in capturing the overall behavior as well as when the configuration was altered.

Keywords: Thermoviscous losses, MEMS microphone, wave-guides

Sammanfattning

Idag är Mikroelektriska mekaniska system (MEMS) mikrofoner är tillgängliga i en rad antal elektroniska konsumentprodukter såsom mobiltelefoner, plattor, smarta klockor och övervakningskameror. MEMS mikrofonen är oftast monterad till ett kretskort med ett hål i som tillåter ljud att propagera genom så väl andra ytterligare ljudguides, vilka kommer att påverka mikrofonens originella frekvensvar. MEMS mikrofonen och andra ljudguides är i samma storleksordnings som dom viskösa och termiska gränsskikten. Dessa är kallade icke-ideala förluster och vanligtvis försumbara för större akustiska system. Det enda sätter att veta påverka av dessa effekter är av att använda finita elementmetoden.

Målet är att inkludera dessa termoviskösa förluster när vågor fortplantar sig genom trånga regioner. System som studeras är Axis Network Camera P1367 och studien fokuserar på den akustiska vägen till mikrofonen. Första målet är att modellera den akustiska vägen tillsammans med MEMS mikrofonen för att producera ett frekvenssvar som matchar det uppmätta frekvenssvaret för olika konfigurationer av den akustiska vägen. Ett andra mål är att hitta den bästa konfigurationen som ger den mest eftertraktade frekvenssvaret.

Flera mätningar gjordes med olika konfigurationer, såsom att variera längden och diametern av hålet i ljudguiden och i kretskortet. Alla mätningar gjordes i ett eko fri kammare. Därefter, en FEM modell var skapad av den akustiska vägen och de olika konfigurationerna som var uppmätta var också simulerade.

Den simulerade frekvenssvaret skilde på vilken frekvens resonansen sker, men de olika konfigurationer av ljudguiden matchar det generella beteendet när man jämför den simulerade och dom uppmätta resultaten.

Den simulerade modellen kräver mer arbete för att uppnå ett simulerat frekvenssvar som matchar den uppmätta, det mest viktigaste är MEMS hålrum. Den riktiga geometrin av MEMS hålrummet gav inte samma frekvenssvart såsom dokumenterad i databladet för denna mikrofonen, då var ett fiktivt hålrum introducerat för att få det önskade frekvenssvaret. Modellen var framgångsrik med att fånga det generella beteendet och var konsistent när ändringar gjordes på den riktiga akustiska vägen.

Nyckelord: Termoviköса förluster, MEMS mikrofon, ljudguide

Acknowledgments

A warm thank you to all the teachers that I've had during my time at BTH, for their inspiration and dedication to their students. I would like to thank Irena Gertsovisch for the initial advice and support for this thesis. I want to thank my supervisor Claes Hedberg for providing informative comments and support. I would like to thank strongly my partner and collaborator for this thesis, Fei Shenyang for his support and positive attitude.

In Axis, I would like to thank Johan Sunnanväder for the constant support and help throughout this thesis. As well as, the other employees at Axis Communications that were always enthusiastic to help.

A special thanks to my classmates from the Master's Program for making my time at BTH that much more enjoyable. And a final thanks to my fellow thesis workers, Zhou Zhuohang, Carlos Tormo, Steve Darmadi and Martin Nilsson at Axis Communication whom provided me with interesting discussions and activities.

(*This page is left blank intentionally*)

Nomenclature

Roman Symbols

Symbol	Description	Units
c	Speed Of Sound	m/s
C_p	Heat Capacity At Constant Pressure	J/K
k	Thermal Conductivity	W/(mK)
p	Pressure	N/m^2
p_0	Ambient Pressure	Pa
T_0	Ambient Temperature	K
Pr	Prandtl Number	1

Greek Symbols

Symbol	Description	Units
α_0	Thermal Expansion Coefficient	K^{-1}
ρ_0	Ambient Density	kg/m^3
β_T	Isothermal Compressibility	Pa^{-1}
δ_{therm}	Thickness Of Thermal boundary layer	m
δ_{visc}	Thickness Of Viscous boundary layer	m
γ	Ratio Of specific heats	1
μ	Dynamic Viscosity	$Pa \cdot s$
μ_B	Bulk Viscosity	$Pa \cdot s$

Contents

List of Figures

List of Tables

Chapter 1

Introduction

1.1 Introduction

This thesis explores and investigates different occurring acoustical phenomena in the camera products of Axis for the purpose of improving the frequency response. If these acoustic phenomena can be found and documented, they can be altered so that the frequency response is changed to a flatter response and removing unwanted amplification and attenuation in the human audible frequency range. There are several reasons why it is desired to obtain a flat frequency response.

1.1.1 Frequency Response

Intelligibility

A frequency response containing strong amplification and attenuation in certain frequency ranges causes loss in Intelligibility. In severe situations even regular conversation could be distorted as a result.

Loss of Information

Due to mechanical design of the MEMS microphone there will be frequencies that are attenuated and amplified. Frequencies that are recorded with the same frequency as the Helmholtz resonance will be amplified and will saturate the system. If the signal is attenuated below the noise floor it will disrupt the incoming information.

Distance Determination

If there is to be an algorithm with the purpose of identifying sounds from a reference sound bank to determine the distance from the sound source to the camera, the algorithm will be erroneous because of incorrect interpretation of signal amplitude data.

Exceptions

There are scenarios where a gain in high frequency amplification could be beneficial. Higher frequencies are attenuated more easily by impeding obstacles. In a situation where the camera is impeded by an obstacle which attenuates high frequencies it would prove beneficial for the system to amplify them.

1.1.2 Research Questions

- What kind of acoustical phenomena occur during the capture of audio by the surveillance camera through its sound-guide and into the MEMS microphone and how can it be modeled in the simulation software to represent an accurate frequency response?
- Can the geometrical features of the acoustic path into the microphone be modified to produce a more desirable frequency response?

1.1.3 Problem Statement

There is a need to improve the acoustic design in surveillance cameras. In audio systems for some applications it is essential to produce a flat frequency response or a more desirable frequency response depending on the application. The acoustic path to the MEMS microphone needs to be investigated to achieve this, as well as understanding the different effects that occur during the capture of sound.

1.1.4 Hypothesis

The acoustical phenomena are found and a simulated model can be built to match the experimental results. As well as, the acoustic path can be modified in such a way to produce a more desirable frequency response for the studied camera.

1.1.5 Limitations

The lack in processing power put restriction on the complexity of the finite element model and thus restricting the accuracy of the simulated model.

1.1.6 Axis Communications

Axis Communications is a company that focuses on the research and development of network surveillance cameras. It's main Research and Development facility is situated in Lund.

1.1.7 Acoustics Path

This thesis looks at the acoustical path that leads the incoming sound from the environment into the microphone. The MEMS microphone has an inherent resonance frequency known as the Helmholtz resonance where the sound inlets neck and the cavity of the front chamber causes this to occur. The microphone is often soldered onto a Printed Circuit Board (PCB) which alters the frequency response as well as any additional wave-guides added to the acoustic path. Because the dimensions of the acoustical path is of the same order of magnitude as the boundary layers they have to be taken into account when performing simulations of the system[2].

1.1.8 Surveillance Camera

The surveillance camera used for this study is the AXIS P1367 network camera and weighs 750 g. The dimensions of the camera are 213 x 80 x 58 mm. In the figure 1.1 below the camera can be seen as well as the sound inlet.

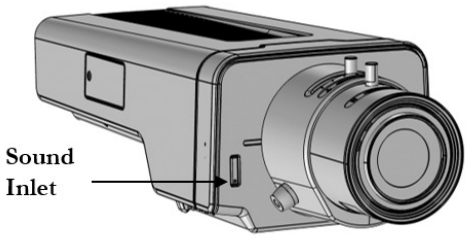

Figure 1.1: The camera AXIS P1367 network camera model, indicating where the sound-guide is located.

1.1.9 MEMS Microphone

For the camera, a specific Micro Electrical Mechanical Systems (MEMS) microphone is used, the INMP522 from InvenSense[1]. The INMP522 is a bottom-port, which means that the sound inlet is located at the substrate versus instead at the package lid, which are then called top-port, see figure 1.2. The package used is a 4 x 3 x 1 mm configuration.

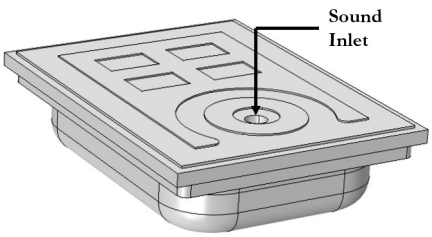

Figure 1.2: A bottom-port MEMS microphone model, indicating where the sound inlet is located.

Chapter 2

Acoustics

2.1 Acoustic Theory

A sound wave is considered a longitudinal wave. Sound waves propagate by pressure and density variation in the air. When a person speaks the vocal tract vibrates and thus displaces the air particles from their equilibrium state and causes them to oscillate. The distinction of the particle velocity and wave velocity should be made clear, particle velocity is the velocity at the air particle is oscillating around an equilibrium and wave velocity is the velocity at which the wave propagates through a medium.
Sound is measured using a standard reference pressure which depends on the medium it propagates through. Because of the wide variation in the magnitude of the different sounds the logarithmic scale is used with the intent to compress the range. Sound pressure level is the most widely used level for measuring sound. For sound pressure level (SPL) the RMS pressure is measured with regards to a reference pressure p_{ref} which is 20 μPa in air and which is also the threshold for hearing (0 dB). Sound pressure level is a dimensionless quantity but is expressed in dB (decibels)[3].

$$SPL = 20log_{10}\left(\frac{P_{RMS}}{P_{REF}}\right) \tag{2.1}$$

2.1.1 Wave Equation

Acoustical waves occur because of pressure fluctuations in the surrounding air and regions of air that is expanding and compressing. To obtain the linear wave equation from the mass, energy and momentum conservation laws, several assumptions are made to produce the linear version of those equations. The linear wave equation is propagating through an inviscid medium which means any dissipative effects caused by viscosity shear and thermal conduction are neglected. The linear wave equation is limited to waves of relatively small amplitude compared to the equilibrium value. [4]

$$\boxed{\nabla^2 p = \frac{1}{c^2}\frac{\partial^2 p}{\partial t^2}} \tag{2.2}$$

2.1.2 Acoustic Resonance

Close-End Tube

In a closed end tube the resonance frequencies will occur when the tube is of a certain length. For its fundamental resonance frequency the ratio of the speed of sound and four times the length of the tube $L = \frac{\lambda}{4}$. The following harmonics are odd integer multiples of the fundamental frequency. The waves traveling inside the tube will have a maximum pressure at the closed end and a minimum pressure at the open end and follow the equation

$$f_n = \frac{nv}{4L}, \tag{2.3}$$

where L is the length of the tube, v is the velocity of sound and n is an odd number $n = 1, 3, 5 \ldots$.

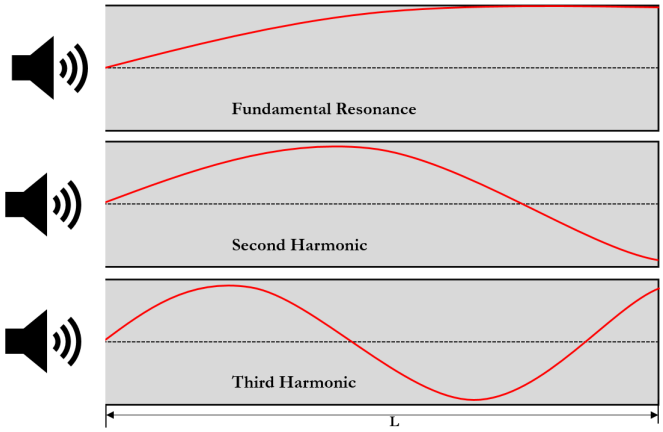

Figure 2.1: The pressure distribution at the fundamental resonance and the two following harmonics.

Open-End Tube

Similar to the close-end tube the resonance frequency depends on the wavelength and the length of the tube. The wave length is now equal to two time the length of the tube, $L = \frac{\lambda}{2}$.

$$f_n = \frac{nv}{2L}, \tag{2.4}$$

where n is a positive integer $(n = 1, 2, 3 \ldots)$

End Correction

In reality the pressure at the openings will not equal to zero because of air radiating into the ambient air causing the wave to reflect back a distance outside the pipe. This distance is called the end correction factor and it depends on the radius of the tube. The larger the tube the larger the end correction factor becomes. Thus

the effective length is introduced to account for this phenomena and it is the sum of the length of the tube and the end correction factor[3]. For unflanged pipes this equals to

$$\Delta l = 0.6133r, \tag{2.5}$$

where r is the radius of the tube.
When modeling a Helmholtz resonator same reasoning applies; an end correction factor is applied. Usually the end of the pipe connected to the chamber cavity is assumed to have an infinite flange which will result in limiting the radiation [3]. The end correction for an infinite flanged tube is given by

$$\Delta l = 0.85r \tag{2.6}$$

Helmholtz Resonance

In figure 2.2 there is a chamber cavity with a narrow neck that has a smaller cross-section. If there is some excitation near the neck this will force the air particles located at the neck to oscillate, creating a pressure difference in the chamber. This can be seen analogous to the spring-mass system where the mass corresponds to the particles located in the neck and the spring is the fluid existing in the chamber [5].

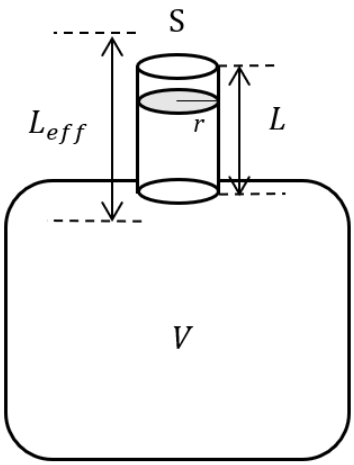

Figure 2.2: A Helmholtz resonator with a narrow circular neck with the cross-section S and a chamber volume V.

The Helmholtz resonance is given by the Eq. (2.7) [3]

$$f = \frac{c}{2\pi}\sqrt{\frac{S}{VL_{eff}}} \tag{2.7}$$

where c is the speed of sound, S is the cross-section of the neck, r is the radius of the neck, L_{eff} is the effective length of the neck which uses the correction factor given in Eq. (2.6) and V is the volume of the chamber.

Acoustic Modes

Usually, the first resonant frequency is of interest in most engineering applications. But in FEM simulation other resonant frequencies can be seen with smaller amplitudes. Each resonant frequency corresponds to an acoustic mode. There are circumferential modes and radial modes. The higher order modes can only be obtained by the use of Finite element method[6].

Cavity Geometry

The geometry of the cavity from an Helmholtz resonant does impact the resonance frequency even though possessing the same volume[7].

2.1.3 Womersley Number

It is practical to consider the thickness of the boundary layer compared to the physical dimensions of the model, the viscous boundary layer δ_v for instance compared to the tube radius a. This is known as the Womersley number which is a dimensionless number used in biofluid mechanics[8].

$$Wo = \sqrt{\frac{\omega \rho a^2}{\mu}} = \frac{a\sqrt{2}}{\delta_v} = \frac{a}{\delta_t}\sqrt{\frac{2}{Pr}} \tag{2.8}$$

Inserting the values for the radius of the tube and the viscous boundary thickness at 1 kHz the following result is obtained

$$Wo = \frac{a \cdot \sqrt{2}}{\delta_v} = \frac{0.125 * 10^{-3} \cdot \sqrt{2}}{0.071 * 10^{-3}} \approx 2.5$$

If the Womersley number is $Wo \ll 1$ then the velocity profile will take the shape of a parabola where the viscous boundary layers will dominate, while if the Womersley number is $1 \ll Wo$ then the velocity profile takes the shape of a plug. Typically if the Womersley number is $Wo < 0.1$ the losses associated with the viscous boundary layer can be disregarded[8].

2.1.4 Propagation in Dissopative Fluids

Thermoviscous Acoustics

In the derivation of the linear wave equation it was assumed that the fluid was adiabatic, meaning that compressions and rarefactions took place without the gain or loss of heat. In fact all media conduct heat to some extent. The existence of heat flow causes reduction of available energy for propagation of the acoustical wave, thus representing an acoustical loss[3]. The fluid is also no longer considered inviscid and thus give rise to velocity gradients which in turn causes viscosity shear near the wall of the pipe.

When the dimensions of the geometry through which the acoustical wave is propagating are narrow enough or contains sharp edges, the losses caused by viscous shearing and thermal conduction need to be taken into account to enable the creation of an accurate model to match the experimental measurement. The consequence of thermoviscous losses is most prominent for the resonance peak in the frequency response. The resonances will often shift down in frequency and broaden[2].

Boundary Layers

Acoustical waves that propagate through narrow regions bounded by walls have viscous and thermal boundary layers forming near the wall surface. The velocity field at the boundary wall is zero because of the viscous resistance to velocity change depicted in figure 2.3. It is no longer assumed that the fluid is inviscid which would avoid the viscous losses altogether but now the temperature is isothermal because the heat conduction of solids are of magnitudes higher than that of fluids but adiabatic in the bulk. It is important to mention that not all of the dissipation occur at the boundaries but occurs in the bulk as well[2].

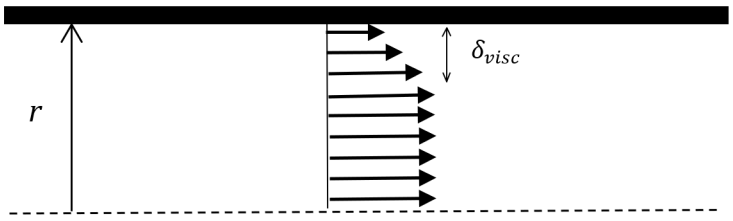

Figure 2.3: The figure showing the velocity gradient losses caused by the boundary layers at the rigid wall due to viscous shearing.

This presence of a viscous boundary layer causes it to have a thickness. The thickness of the viscous boundary layer is

$$\delta_{visc}^{BL} = \sqrt{\frac{2\mu}{\omega\rho_0}} \tag{2.9}$$

where μ is the dynamic viscosity which is a measure of a fluid's resistance to shearing, ω is the angular frequency and the ρ_0 is the equilibrium density.

Concurrent with the viscous boundary layer is a thermal boundary layer for which the fluid at the pipe walls is no longer assumed to be adiabatic and is instead assumed isothermal because the thermal conduction is several magnitude larger in solids than in fluids. At the mainstream of the fluid it is still assumed adiabatic[3]. The thermal boundary layer thickness δ_{therm}^{BL} is given by

$$\delta_{therm}^{BL} = \sqrt{\frac{2k}{\omega \rho_0 C_p}} \tag{2.10}$$

where k is the thermal conductivity and C_p is the isobaric heat capacity. The viscous boundary layer and the thermal boundary layer are related by the so called Prandtl's number

$$Pr = \frac{C_p \mu}{k} \tag{2.11}$$

$$\delta_{visc} = \delta_{therm} \sqrt{Pr} \tag{2.12}$$

This ratio gives a measure for how much of the losses are because of viscous losses or thermal losses, for air the Prandtl number is 0.7 which indicate an almost equal importance[2].

In figure 2.4 the thermal and viscous boundary layers thicknesses are plotted over the audible frequency range. At 1 kHz the thermal and viscous boundary layer thicknesses are 0.084 mm and 0.071 mm respectively.

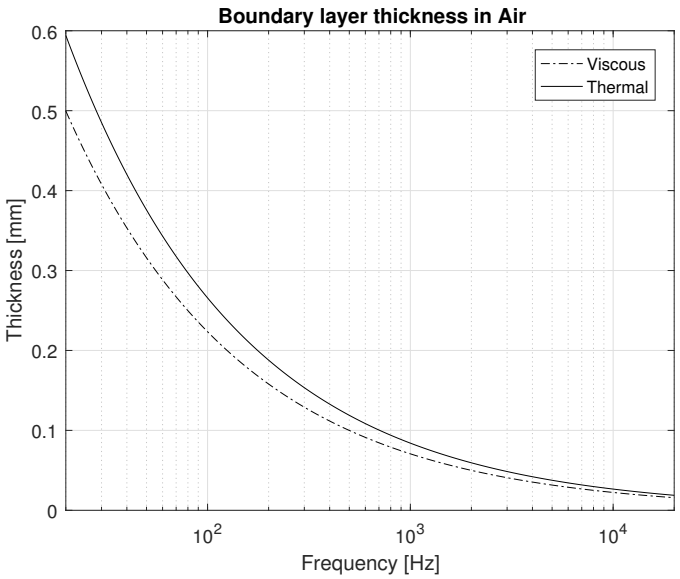

Figure 2.4: The plot showing the thermal and viscous boundary layer thickness over the audible frequency range for air

General Thermoviscous Regime

The linearized versions of the continuity, momentum (Naiver-Stokes) and the energy equation as well as the state equations for and ideal gas are obtained by assuming small perturbations around an equilibrium or steady background properties[8]. For the time-harmonic case given by the angular frequency $\omega = 2\pi f$ the perturbations are expressed as the following

$$p = p_0 + p'e^{i\omega t} \tag{2.13}$$

$$\mathbf{u} = \mathbf{u}_0 + \mathbf{u}'e^{i\omega t} \tag{2.14}$$

$$T = T_0 + T'e^{i\omega t} \tag{2.15}$$

where primed variables $p'e^{i\omega t}$, $\mathbf{u}'e^{i\omega t}$, $T'e^{i\omega t}$ are the perturbed quantities of pressure, velocity field and temperature respectively and p_0, $\mathbf{u}_0$ and T_0 are the ambient pressure, velocity field and temperature respectively[2].

The equations are solved in time domain and converted into frequency domain from time domain by the relation

$$\frac{\partial}{\partial t} = -i\omega \tag{2.16}$$

The following equations govern the physics in the Thermoviscous module in COMSOL Multiphysics. Equation (2.17) is the linearized continuity equation. (Further primed notations are omitted)

$$i\omega\rho = -\rho_0(\nabla \cdot \mathbf{u}) \tag{2.17}$$

where ρ_0 is the ambient density. The momentum equation (2.18) is given by

$$i\omega\rho_0\mathbf{u} = \nabla \cdot \left(-p\mathbf{I} + \mu(\nabla\mathbf{u} + (\nabla\mathbf{u})^T) + \left(\mu_B - \frac{2}{3}\mu\right)(\nabla\mathbf{u})\mathbf{I}\right) \tag{2.18}$$

where μ and μ_B is the dynamic and bulk viscosity respectively. The energy conservation equation (2.19)

$$i\omega(\rho_0 C_p T - T_0\alpha_0 p) = -\nabla \cdot (-k\nabla T) \tag{2.19}$$

where k , C_p and α_0 is the thermal conductivity, heat capacity at constant pressure and thermal expansion coefficient at constant pressure respectively[8].

The final equation (2.20) is the linearized equation of state which contains the relations between pressure, density and temperature variations

$$\rho = \rho_0(\beta_T p - \alpha_0 T) \tag{2.20}$$

and where β_T is the isothermal compressibility.

Chapter 3

Microphone

3.1 Theory

3.1.1 MEMS microphones

MEMS sensor

A MEMS (Micro-Electrical-Mechanical-System) sensor is basically a silicon capacitor. The sensor consists of a back-plate and a front-plate. The fixed and rigid back-plate is filled with acoustical holes which let sound pass through and is covered by an electrode layer while the front-plate (membrane) is flexible and only fixed at one end. The MEMS sensor is a capacitive transducer where the change in amount of capacitance is caused by the movement of the flexible plate by incoming sound waves.
Figure 3.1 shows the typical structure of a MEMS sensor. A ventilation hole is present to let the compressed air exit the chamber, concurrently enabling the membrane to move back[9].

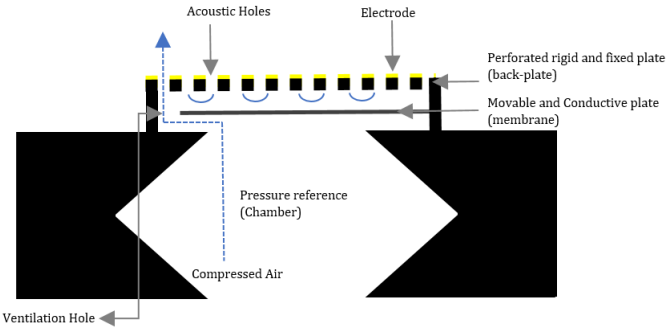

Figure 3.1: The MEMS sensor showing the interaction between the rigid and fixed plated and the flexible conductive plate.

ASIC

The ASIC or Application Specific Integrated Circuit exerts a constant charge on the membrane of the MEMS sensor. The ASIC measures the voltage changes when the membrane is displaced by incoming sound waves because of the change in capacitance and translates that into an electrical signal [10].

Packaging

The MEMS microphone components are usually attached to a substrate which are then covered by a packaging lid. On the other side of the substrate, solder pads are present, which can be soldered onto a Printed Circuit Board (PCB) or a flex circuit. The packaging of the MEMS sensor as well as the ASIC determines the Signal-to-Noise ratio and the frequency response.
There are two configurations of the MEMS microphone, top-port and bottom-port packaging. For top-port microphones the sound inlet is located on the packaging lid, and for this configuration the lid package cavity becomes the front chamber and the MEMS sensor cavity the back chamber[9].

The consequences of these packaging configurations shown in figure 3.2 are that the large front chamber causes a Helmholtz resonance in the audible range in the frequency response, and that the small back chamber restricts the responsiveness of the membrane and thus lowering the Signal-to-Noise ratio[9].

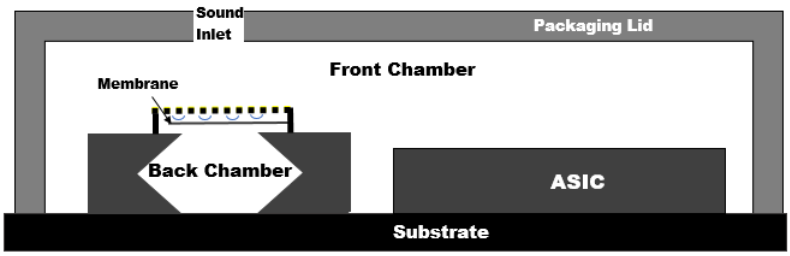

Figure 3.2: The cross-section of MEMS microphone showcasing the sound inlet located at the package lid.

The consequences of a bottom-port packaging configuration shown in figure 3.3 are that the small front chamber causes that the Helmholtz resonance to occurs outside the audible range in the frequency response, and the large back chamber increases the responsiveness of the membrane and thus improving the Signal-to-Noise ratio. The disadvantage that the bottom-port microphones have is that the sound inlet is on the surface that will be soldered on to a PCB or a flex PCB, thus during the soldering process unwanted contamination might enter the sound inlet and damage the sensor. Meanwhile, the top-port microphones avoids this issue completely[9].

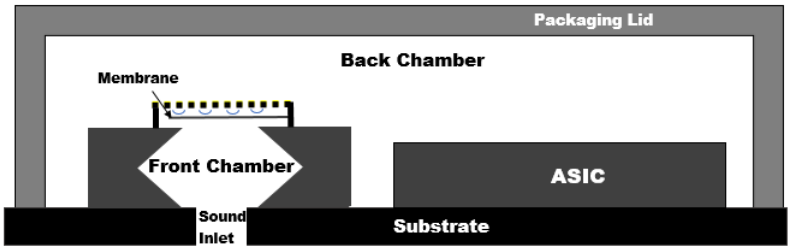

Figure 3.3: The cross-section of MEMS microphone showcasing the sound inlet over the sensor at the substrate.

InvenSense INMP522

The camera is using the bottom-ported MEMS microphone INMP522 from InvenSense. When inspecting the specification sheet and observing the frequency response of the INMP522 there is low frequency roll of at the -3 dB point and a resonance frequency at 12 kHz with an amplitude of 8 dB[1].
This resonance is caused by the volume in the front chamber and the neck of the substrate forming a Helmholtz resonator. In figure 3.4 the frequency response is shown.

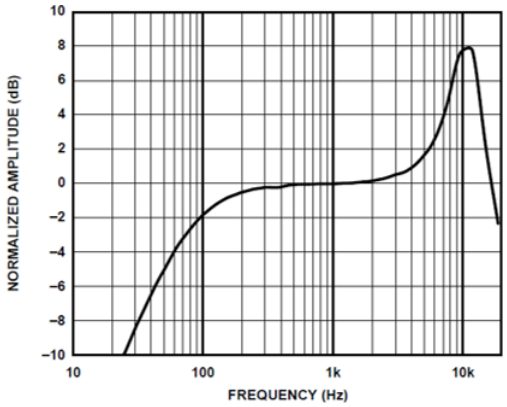

Figure 3.4: The frequency response of the MEMS microphone given by the data-sheet form the manufacturer[1].

3.2 Microphone Specifications

3.2.1 Sensitivity

The sensitivity of a microphone is defined as the ratio between an acoustical input and the analog voltage and is measured in for an analog microphone mV/Pa and usually expressed in dB by using

$$Sensitivity_{dBV} = 20log_{10}\left(\frac{Sensitivity_{mV/Pa}}{Output_{REF}}\right), \tag{3.1}$$

where $Output_{REF}$ is the 1V/Pa reference output ratio.
For a digital microphone the sensitivity is measured as the percentage of the full scale output that is generated by a 94 dB SPL input[11]. The conversion equation is

$$Sensitivity_{dBFS} = 20log_{10}\left(\frac{Sensitivity_{\%FS}}{Output_{REF}}\right) \tag{3.2}$$

3.2.2 Directionality

Directionality of a microphone describes how the sensitivity varies with changing position of sound source in space. It is measured as a function of angle and amplitude and is appropriately plotted in a polar graph. A desirable characteristic of a microphone is omni-directionality which the INMP522 microphone possesses, which implies invariant sensitivity with changing angle, regardless of the orientation of the microphone. Although, when contained in a product housing this characteristic is often not maintained[11].

3.2.3 Equivalent Input Noise

Equivalent input noise (EIN) is the noise produced by the microphone because of thermal noise or random diaphragm movement and can be viewed as a theoretical input to a noiseless microphone, expressed in dB SPL. The following formulas are used to determine the EIN[11].

$$EIN = Acoustic\ Overload\ Point - Dynamic\ Range \tag{3.3}$$

$$EIN = 94\ dB - SNR \tag{3.4}$$

3.2.4 Dynamic Range

Dynamic range is the difference between the largest amplitude and the power of the noise floor. In the dynamic range the microphone responds linearly up until the Acoustic overload point is reached, which is usually at 120 dB[11]. The dynamic range for a MEMS microphone is given by the difference of the acoustic overload point (AOP) and the Equivalent input noise (EIN)

$$DynamicRange = AOP - EIN \tag{3.5}$$

3.2.5 Frequency Response

The frequency response is a measure of the output spectrum in response to an input and the output is a measure of magnitude and phase as a function of frequency. The reference level at 1 kHz is customarily normalized at 0 dB. For audio systems the goal is often to recreate the captured signal without any distortions i.e. possessing a uniform magnitude of response (flat frequency response)[11].

3.2.6 Total Harmonic Distortion

When a pure tone signal is used as an input to the system, total harmonic distortion (THD) gives a measure in percent of the distortions caused by non-linearites in the system. It is defined as the ratio between the sum of the power of all the harmonics and the power of the fundamental frequency[11].

$$THD = \frac{\sum_{n=1}^{\infty} Power(f_{harmonics_n})}{Power(f_{fundamental})} \tag{3.6}$$

3.2.7 Acoustic Overload Point

The Acoustic overload point (AOP) is the SPL at which the input signal reaches 10 % THD, signals beyond that point are no longer represented linearly by the microphone[11].

Chapter 4

Related Work

4.1 Acoustic Analysis of Loudspeaker Cavity Including Viscothermal Effects

Boel Hökmark's Master's thesis paper gives informative introduction of the thermoviscous losses that occur when acoustical waves propagate through narrow ducts or sharp corners [5]. Boel concludes that for more accurate results both thermal and viscous losses must be included. As a simulation tool Boel used ABAQUS which was not equipped to include the non-ideal losses in a manageable way and also it does not include thermal losses.

4.2 A Microacoustic Analysis Including Viscosity and Thermal Conductivity to Model the Effect of the Protective Cap on the Acoustic Response of a MEMS Microphone

In this paper the MEMS microphone is studied [12]. This paper proves that including the thermoviscous losses in the wave equation is imperative to obtain simulated results that match the measured results because the boundary layers that form when waves propagate in narrow regions are in the same magnitude as the geometry. To obtain a correct simulated sound pressure distribution viscous shearing need to be included and to simulate the correct amplitude of the resonance peak caused by the Helmholtz resonance thermal conduction needs to be included.

4.3 Gasket Design for Optimal Acoustic Performance in MEMS Microphones

This technical report investigates the geometrical effect of the gasket to the frequency response [13]. In this investigation the length and thickness of the gasket is varied to investigate how it alters the Helmholtz resonance caused by the MEMS microphone. This technical report also shows simulations of more complex gasket geometries to further see how it affects the frequency response. This study is lacking the application of thermoviscous losses that occur when waves propagate through small geometries which will have a significant impact on the frequency response.

4.4 Development of a General Acoustics Model for an Arbitrary Camera Design

This thesis focuses on the simulations of the acoustical path to the MEMS microphone[14]. More complex geometries of the gasket are studied, such as a tortuous path to the MEMS microphones but without the thermoviscous effects.

Chapter 5

Method

5.1 Measurements

5.1.1 An-echoic Chamber

The purpose of an an-echoic chamber is to simulate free-field conditions or an infinitely large room where the reverberations are kept to a minimum so the reflecting waves cause less interference. The an-echoic chamber used for this work is a non-certified custom built full an-echoic chamber, which means it dissipates the energy of acoustical waves in all directions, see figure 5.1. Each wall has half of meter of padding material and is covered by an acoustic wedge.

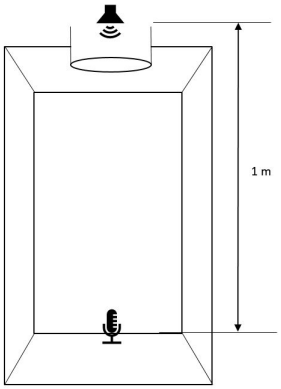

Figure 5.1: Figure showing the an-echoic chamber

The an-echoic chamber has also a built-in laser assisting calibration. The three lasers beams in the chamber intersect to form a point where the microphone sound inlet should be placed during compensation and measurements.

5.1.2 Measurement Equipment and Setup

The following measurement tools were used for the acquisition of data.

- Earthworks M30 Calibration microphone
- Manfrotto 244RC Variable Friction Magic Arm (Camera/Mic Stand)
- SpectraPLUS FFT Spectral Analyzer Software
- Behringer iNUKE NU1000 Power Amplifier
- M-Track Plus II
- AXIS P1367 Network Camera
- Ethernet cable
- XLR Microphone Male to Female Audio Cable
- MEMS microphone INMP552
- Speaker Element JORDAN JX92S

Figure 5.2 shows the experimental setup schematic for the calibration using M30 microphone and the camera P1367.

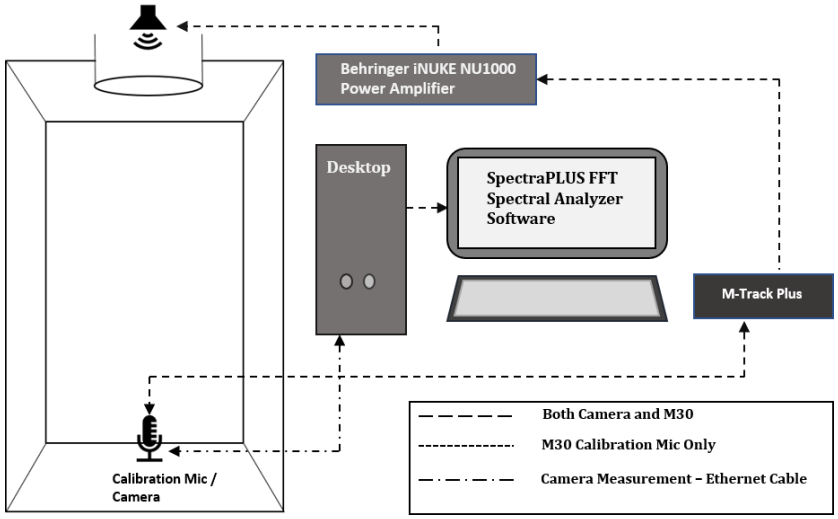

Figure 5.2: Setup schematics

5.1.3 Acoustic Path to Microphone

The audio system consists of a PCB with sound-guide adhered to it. The sound-guide is attached to the camera housing. The dimensions of the sound-guide are shown in the figure 5.3 below. In further text when referring to the original sound-guide this means the sound-guide currently used in the Axis Network camera P1367 which possesses the funnel shape as shown in figure 5.3. The diameter in the sound inlet is 0.6 mm and at the exit it is 0.8 mm. The other two holes are drilled having a diameter of 1 mm and 1.5 mm with a uniform cross-section. Also, a thin adhesive tape used to connect the sound-guide together with the PCB, the thickness of the adhesive is approximately 0.1 mm and thinner when compressed together.

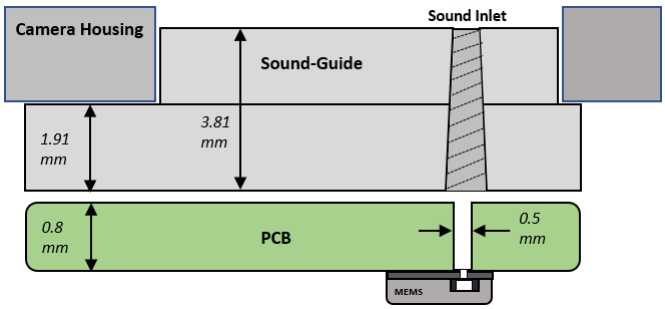

Figure 5.3: Acoustic path to the MEMS microphone

5.1.4 SpectraPLUS setting

In SpectraPLUS FFT Spectral Analyzer Software the following settings were used: a 48 kHz sampling rate, FFT sample size was 16384 samples and a decimation ratio of 1. The spectral resolution was 2.93 Hz. Smoothing window was the Hanning window. For the input signal a logarithmic frequency sweep was used. The sweep ranges from 20 Hz to 21 kHz with the duration of 1 second. The infinite averages options was used. Exported measurement data were always normalized to 0 dB at 1 kHz.

5.2 Finite element modeling

To model the thermoviscous effect COMSOL Multiphysics was used. In COMSOL there are two ways to apply the thermoviscous effect on the model; the first one which is a simplified version and only apply for certain geometries, this option can be found in Pressure acoustics called Narrow region acoustics which is computationally inexpensive. The second way is to select thermoviscous acoustics and apply it to the model domain were temperature, pressure and velocity gradients are solved from the linearized Naiver-Stokes equations[8].

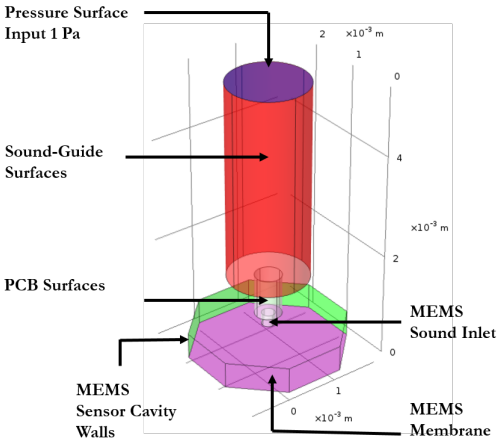

Figure 5.4: The acoustic path leading to the MEMS sensor cavity. The diameter of the sound-guide is 1.5 mm and the cavity geometry is a octagonal prism

Figure 5.4 above shows the model appearance. For this particular model the Sound-guide has a 1.5 mm diameter hole. At the top the pressure is always selected to be 1 Pa. The sensor cavity has the geometry of the octagonal prism which is the real geometry used in the INMP552 of the front-chamber.

Table 5.1 lists all the constants used for the simulation.

Table 5.1: Table of the constants used in the Simulations

Symbol	**Value**	**Unit**	**Description**
T_0	298.15	[K]	Ambient Temperature
p_0	101325	[Pa]	Ambient Pressure
M_{mol}	28.8	[g/mol]	Molar mass of air
R	8.13144621	[J/mol/K]	Ideal gas constant
$r_{air} = R/M_{mol}$	288.6966	[J/kg/K]	Air gas constant
$\rho_0 = p_0/r_{air}/T_0$	1.1772	$[kg/m^3]$	Ambient Density
$\gamma = C_p/C_v$	1.401	[1]	Ratio of Specific heats
C_p	$1.0049 \cdot 10^3$	[J/kg/K]	Specific Heat at constant pressure
k	$2.624 \cdot 10^{-2}$	[W/m/K]	Thermal Conductivity
μ	$1.846 \cdot 10^{-5}$	$[Pa \cdot s]$	Dynamic Viscosity
μ_B	0	$[Pa \cdot s]$	Bulk Viscosity
c_0	343	[m/s]	Speed of sound in Air
$Z_0 = \rho_0 c_0$	408.6414	$[Pa \cdot s/m]$	Acoustic impedance of Air

5.3 Pressure Acoustics

5.3.1 Narrow Region Acoustics

Modeling the acoustic cavities using the Pressure Acoustics module provides a computation inexpensive alternative to model the thermoviscous losses for when waves propagate through circular, rectangular and equilateral triangular ducts as well as for very narrow slits and ducts or wide ducts. The duct type used for modeling the simplified model was of type circular duct. There are conditions that have to be fulfilled in order to achieve the most out of these simplifications. The conditions are that the acoustic wavelength must be much larger than the boundary layers thickness $\delta^{BL} \ll \lambda$, the cross-section must remain uniform or slowly varying cross-section if the length of the tube is sufficient, and that the length of the wave-guide must be smaller than the boundary layer thickness $\delta^{BL} < L$[8].

Figure 5.5 shows the result of the sound-guide with 1.5 mm hole and the PCB with the 0.5 mm hole, and compares the frequency response with Narrow Region Acoustics applied and without. Both results also have impedances applied to the surfaces of the model as shown in figure 5.4 with the values from table 5.2.

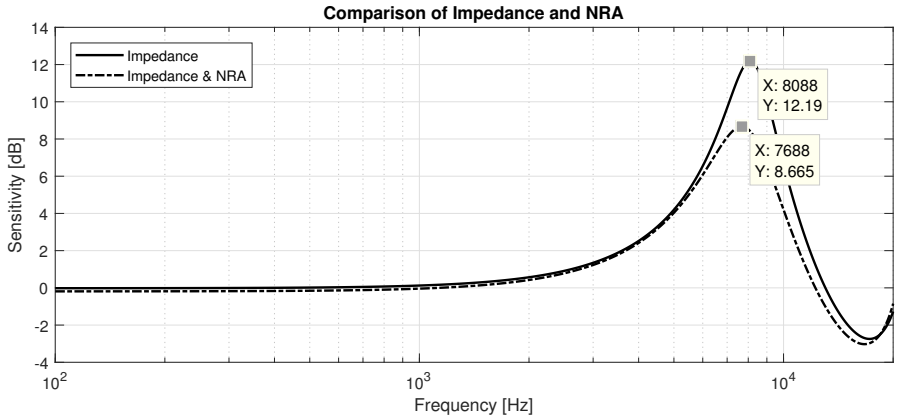

Figure 5.5: The comparison of the frequency response of the 1.5 mm hole with 0.5 mm PCB with and without thermoviscous losses

Table 5.2: The densities and sound velocity in materials used in the model

Material	Density $[kg/m^3]$	Sound velocity in material $[m/s]$
Air	1.177	343
PCB (FR-4)	1850	3600
Silicon	2000	1500
MEMS membrane	120	150
Sound-Guide (PC)	1200	2260

5.3.2 Helmholtz Resonator Cavity Geometries

The resonance frequency of a Helmholtz resonator is dependant on the geometry of the cavity chamber despite having the same volume. In figure 5.6 three cavity geometries are modeled in the Pressure Acoustic module in COMSOL. The first geometry is a truncated pyramid, which is a geometry used in ST top-port microphone MP34DT05. The second one is a cylindrical cavity which is axis symmetric and it is the cavity used to produce the simulation results. And the final cavity is an octagonal prism which was found by manually removing the package lid of the INMP522 MEMS microphone and see the shape through a microscope. The volume of the cavities is V = 3.056 mm^3 and the neck radius and length are 0.125 mm and 0.23 mm respectively.

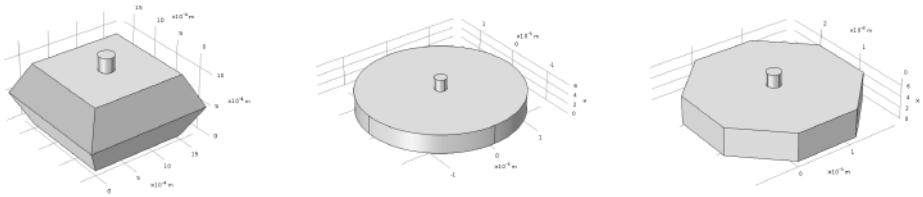

Figure 5.6: The three different cavities of an MEMS sensor with the same volume, neck radius and neck length

The results can be seen in the figure 5.7 which shows that the truncated pyramid cavity has the highest resonance and is 200 Hz higher than the cylinder cavity. The octagonal prism cavity is in between the resonance frequencies of the other two cavities at 12.17 kHz.

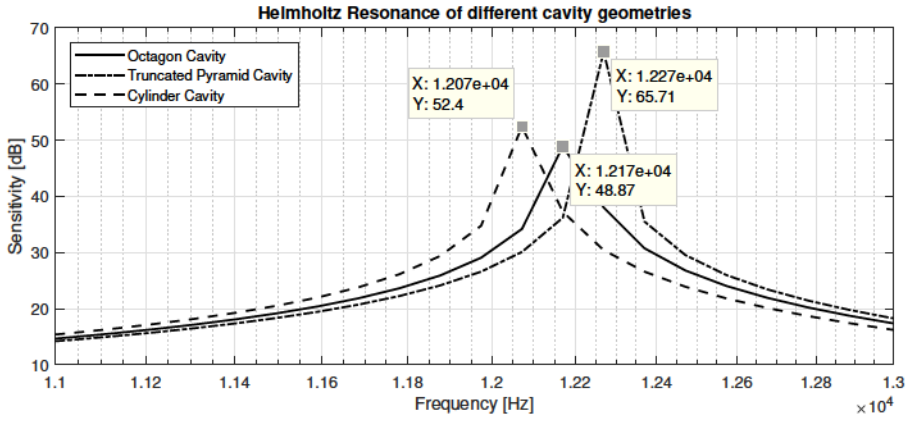

Figure 5.7: The plotted frequency responses of the three different cavities shown in figure 5.6.

5.4 Thermoviscous Acoustics

5.4.1 MEMS Sensor Cavity

The geometry of the front-chamber was obtained by removing the package lid and separating the sensor cavity from the substrate and then use a measuring microscope to obtain the dimensions. The geometry of the sensor cavity in the INMP522 MEMS microphone was an octagonal prism thereafter the volume could be calculated, see figure 5.8. The dimension of the neck in the MEMS microphone was measured as well. The theoretical results gave a resonance that occurred outside the audible frequency range which didn't match the measured frequency response of the INMP522 in the corresponding data sheet[1]. A speculation is that the front-chamber is somehow connected to the back-chamber resulting in a larger cavity volume, consequently decreasing the Helmholtz resonance.

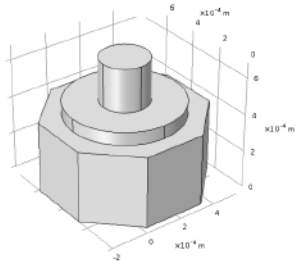

Figure 5.8: The geometry of the real cavity in the INMP522 MEMS microphone

Thus, a fictive cavity was simulated to match the resonance seen in the data sheet at 12 kHz[1]. Because the measured frequency response inherently includes the thermoviscous losses the simulated model included them as well. But it is hard to predict how much the resonance frequency will shift down because of these losses and thus a guessing approach of the volume inside the front chamber cavity was used until the desired resonance frequency could be obtained. The simulated frequency response is shown in figure 5.9 along with the pressure distribution in the cavity at resonance.

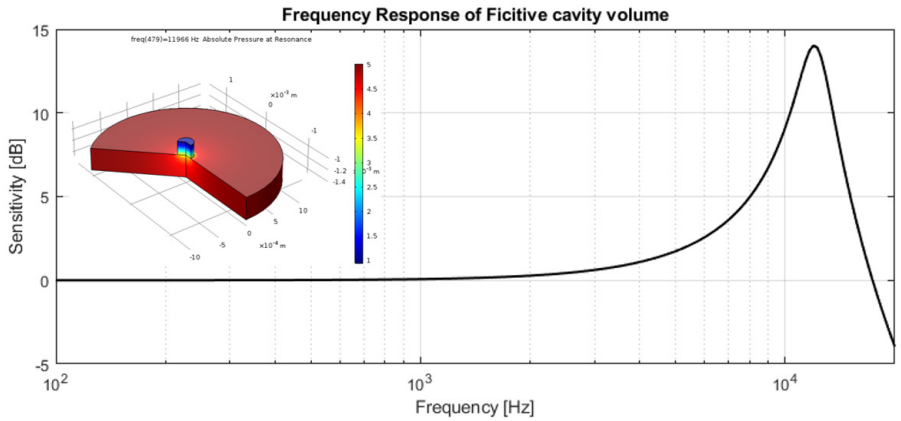

Figure 5.9: The plotted frequency response of the simulated MEMS cavity and the pressure distribution at the resonance that is occurring at 12 kHz

The shape of the fictive cavity is shown in figure 5.10 below. The octagonal shape of the cavity model is omitted and instead a cylindrical cavity is used instead. The reason is because of the cylinders axial symmetry the simulation can be performed in 2D Axis-Symmetric space dimension, saving computational time and making it easier to mesh the boundary layers[15].

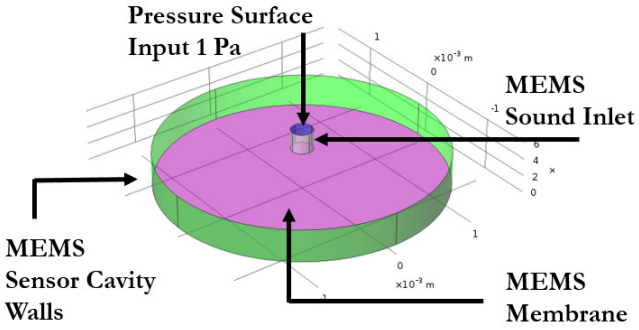

Figure 5.10: The simplified cylinder geometry used in the simulations from here now on.

The three-dimensional model can still be used coupled with the Pressure Acoustics to show the varying resonance frequency for different geometries with the same volume. Three cavities will be used to demonstrate this, the octagonal prism cavity, the truncated pyramid and the cylinder cavity.

The next step is to add the PCB and the sound-guides in the simulation model. Because both geometries of the PCB and Sound-guide hole are axis symmetric the whole simplified model can be simulated in the axis symmetric space dimension to save precious computation time.

5.4.2 Mesh

Modeling the propagation of sound waves requires that the maximum mesh size is one fifth of the smallest wavelength of interest. Also, when modeling in the thermoviscous domain it is essential to have a boundary layer mesh, that is a finer mesh at the edges of the model to capture the changes of the temperature and velocity gradients i.e. the thermoviscous losses. Figure 5.11 shows the mesh used for simulation of the axis symmetric MEMS sensor cavity[15].

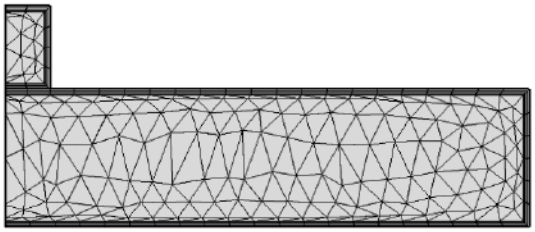

Figure 5.11: Showing the mesh used for the simulation of the cylindrical INMP522 MEMS sensor cavity

Chapter 6

Results

6.1 Measurement Results

6.1.1 Measurement Setups

Figure 6.1 shows the setups used for the conceptual experiments. Setup 1 shows the configuration of the hand made Helmholtz resonator on top of the calibration microphone. Setup 2 shows the configuration of the the sound-guide cut into a circular shape of the same diameter as the head of the calibration microphone. Setup 3 shows the configurations for the interference setup where a rectangular aluminum plate is situated beneath the microphone head along with a hollow cylinder covered by porous material with a thickness of 43 mm.

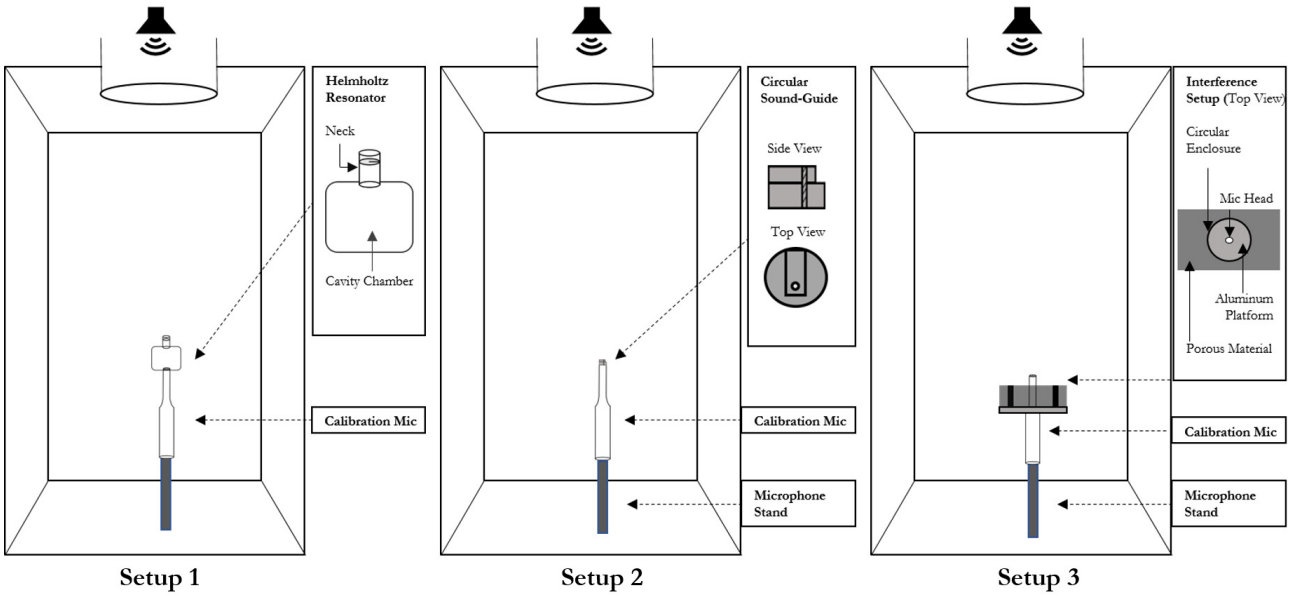

Figure 6.1: The three measurement setups used for the conceptual experiments.

Figure 6.2 shows the two setups used for the investigation of the frequency response of the acoustic path shown in figure 5.3. Setup 4 shows the network camera setup and Setup 5 shows the acoustic path moved outside from the camera. The PCB must be connected to the camera's circuit board for power which is why it can be seen underneath the acoustic path in Setup 5.

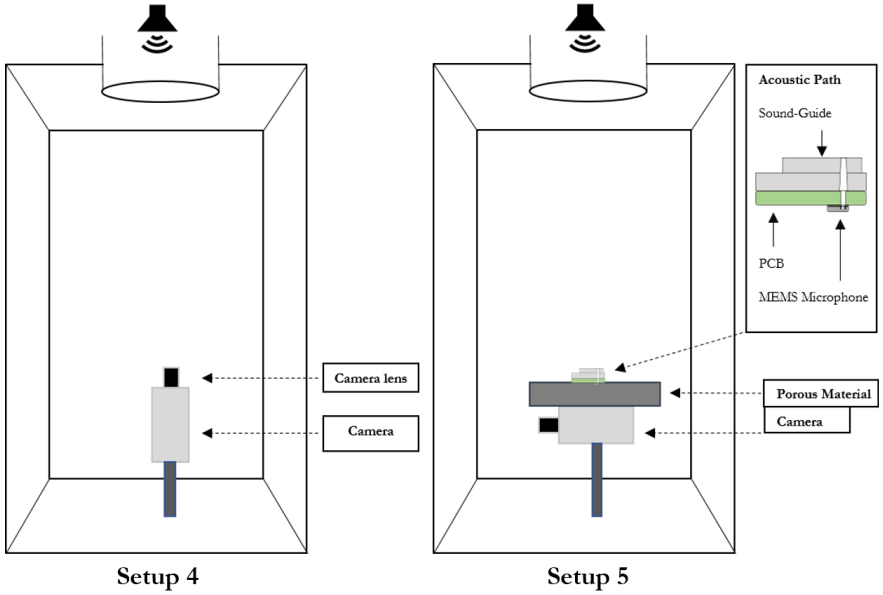

Figure 6.2: The two measurement setup used for the study of the acoustic path.

6.1.2 Conceptual tests

The Earthworks M30 microphone has a flat frequency response in the range 5 Hz to 30 kHz. This microphone is used to calibrate for any unwanted room acoustics.

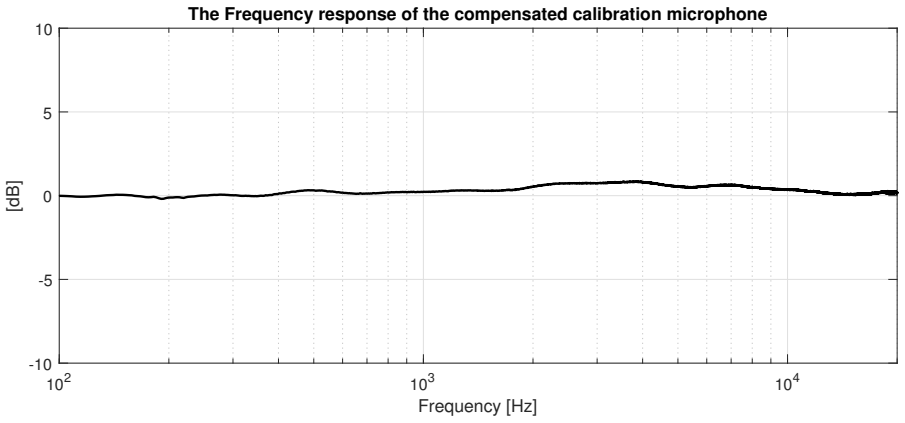

Figure 6.3: The Frequency response of the calibrated microphone.

Quarter wavelength resonator

The acoustic resonance in a closed end tube shown in figure 2.1 where three first resonant frequencies are depicted. The setup used for this is similar to Setup 1 in figure 6.1 but instead a tube of length 77 mm is used. The tube was about the same diameter as the calibration microphone sound inlet, thereafter both were connected by tape.

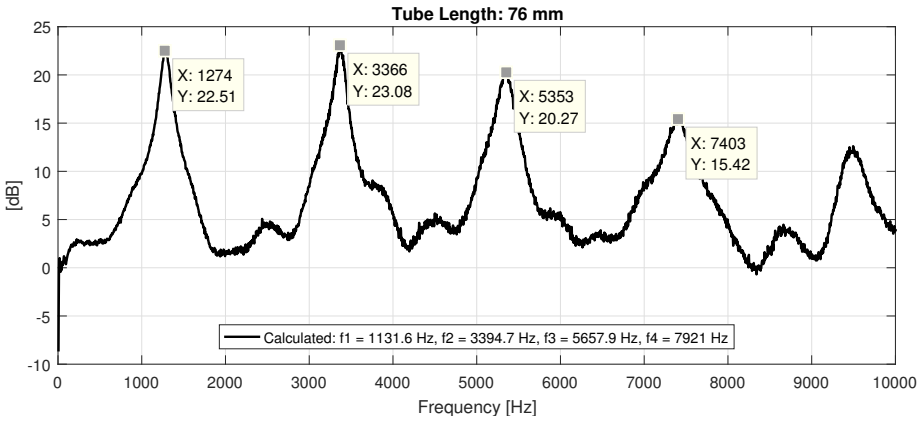

Figure 6.4: The fundamental frequency and the three following harmonics. The legend shows the calculated resonance frequencies.

The theoretical results gives including the end correction factor

$$f_1 = \frac{v}{4L} = \frac{1 \cdot 343}{4 \cdot (77 \cdot 10^{-3} + 0.4 \cdot 9.8 \cdot 10^{-3})} = 1062.8Hz$$

and the second and third harmonics are 3188.3 Hz and 5313.9 Hz respectively.

Helmholtz resonance

The setup used for this experiment is Setup 1 shown in figure 6.1 where a handmade Helmholtz resonator is used. The radius and length of the neck is 4.9 mm and 69.1 mm respectively and the height and radius of the cavity is 48 mm and 17.575 mm respectively.

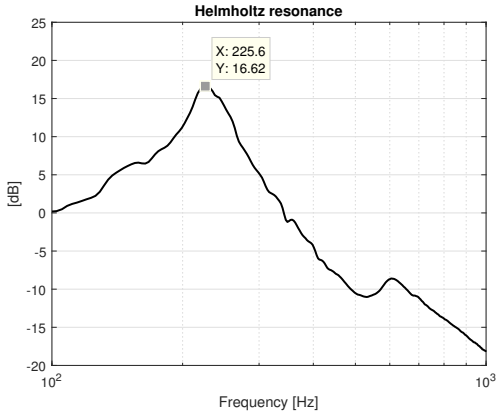

Figure 6.5: Showcasing the Helmholtz resonance in the range of 100 and 500 Hz

Calculating the theoretical resonance with the end correction factor gives.

$$f_r = \frac{c}{2\pi}\sqrt{\frac{S}{V \cdot L_{eff}}} =$$

$$\frac{343}{2\pi}\sqrt{\frac{\pi \cdot (4.9 \cdot 10^{-3})^2}{48 \cdot 10^{-3} \cdot \pi \cdot (17.575 \cdot 10^{-3})^2 \cdot (69.1 \cdot 10^{-3} + 0.85 \cdot 4.9 \cdot 10^{-3})}} = 256.6529Hz$$

In figure 6.5 another smaller peak after the main resonance can be seen. This cannot be calculated by any formula, instead finite element method needs to be used.

Thermoviscous losses

Figure 6.6 shows the measurements results from using the calibration microphone with a circular sound-guide placed on top of the sound inlet, the setup that used for these measurements is Setup 2 shown by figure 6.1. Two hole diameters were used, the dashed results in figure 6.6 uses the original hole(0.6/0.8 mm) and the solid line shows the results of the 1.5 mm hole in the circular sound-guide. To obtain better results an adhesive tape was used to attach the circular sound-guide to the microphones sound-inlet.

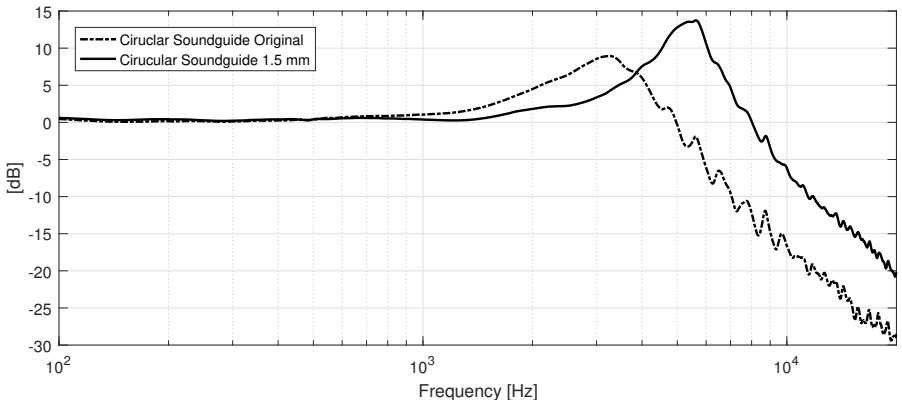

Figure 6.6: The comparison of the sound-guide on top on the calibration microphone for two different hole diameters.

Figure 6.6 shows that increasing the diameter of the sound-guide hole reduces the thermoviscous losses, this results in a resonance with a higher Q-value, and the resonance occurring at a higher frequency. This follows the behaviour described in Propagation in Dissopative Fluids, that thermoviscous losses broaden the peak and shift the resonance down in frequency.

Interference

The measurement results shown in figure 6.7 where Setup 3 is used shown by figure 6.1. Figure 6.7 shows two measurement results, the dashed line is where a aluminum plate with a hole in the middle of it, so that it fits over the calibration microphone and lowered 49 mm below the sound inlet. The second solid line is similar to the first but with an added cylinder to enclose the microphone sticking out of the plate, the diameter of the cylinder is 73 mm.

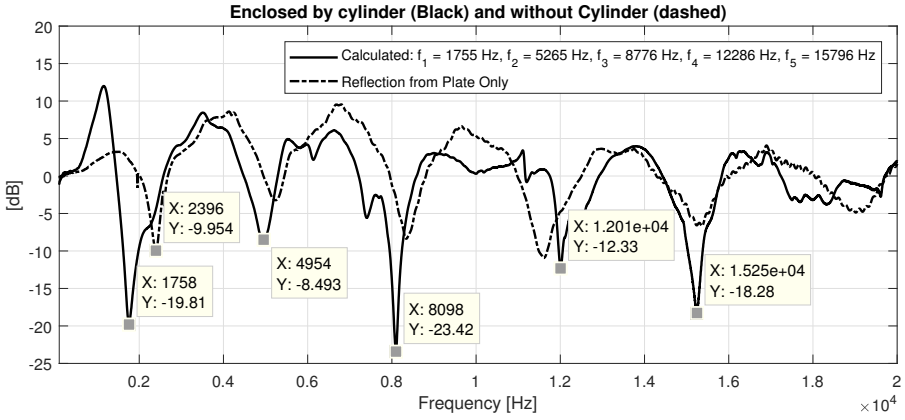

Figure 6.7: The fundamental frequency and the three following harmonics and in the legend showing the calculated resonance frequencies.

The formula for the closed-end tube was used to obtain the theoretical results of where what frequencies would the anti-resonance occur, where L = 49 mm. The theoretical calculation matched the first measurements well except for the first anti-resonance. When the cylinder was added the first anti-resonance matched better with the theoretical calculations. For the measurement with the cylinder the Q-factor is higher than for the one without the cylinder, which could be because less reflections occur when a cylinder is present.

6.1.3 Fully Assembled Camera

Figure 6.8 shows the original sound-guide used in the Axis network camera P1367. The diameter at the entrance of the sound-guide is 0.6 mm and at the exit 0.8 mm. The figure shows a resonance around 7195 Hz with an amplitude of 17.37 dB. The setup used for the following measurements as shown by Setup 4 in figure 6.2.

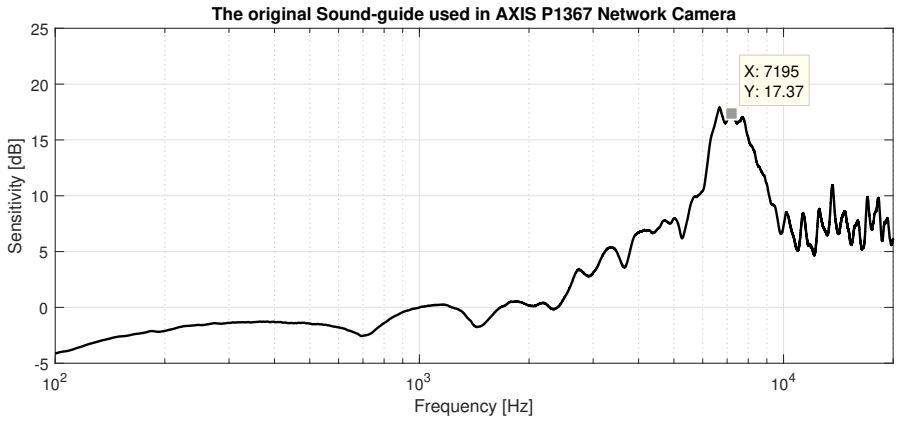

Figure 6.8: This plot shows the frequency response of the original sound-guide in the camera housing.

6.1.4 Assembled Camera without Lens

Figure 6.9 shows the comparison of camera with and without camera lens for the original sound-guide. The effect of having no lens seem to have is that it slightly broaden the resonance peak and gives rise to a slight attenuation after 10 kHz.

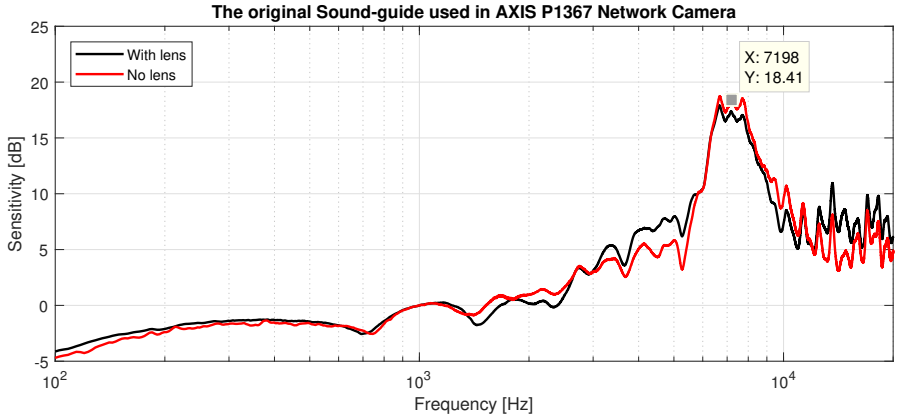

Figure 6.9: This plot compares the Frequency responses of the camera with and without lens for the sound-guide with 0.6/0.8 mm diameter hole.

Figure 6.10 shows the comparison of camera with and without camera lens for the 1 mm sound-guide diameter hole. The effect that having no lens is that it slightly broadens the resonance peak and gives rise to a anti-resonance at around 16 kHz.

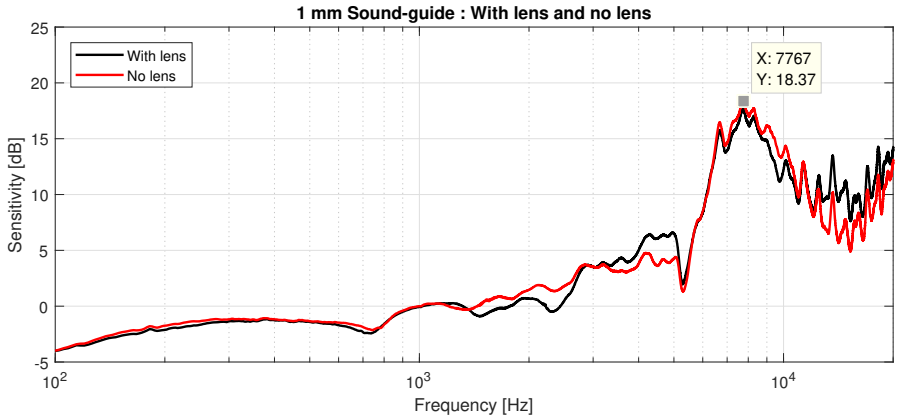

Figure 6.10: This plot compares the Frequency responses of the camera with and without lens for the modified sound-guide with 1 mm diameter hole.

Figure 6.11 shows the comparison of camera with and without camera lens for the modified sound-guide with 1.5 mm diameter hole. The effect of having no lens is that it slightly amplifies a small range before the resonance frequency but maintains the same behaviour as with the lens afterwards.

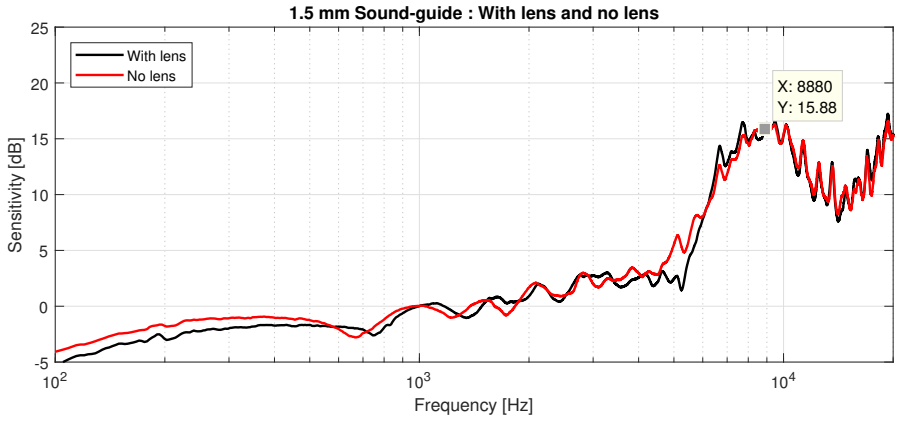

Figure 6.11: This plot compares the Frequency responses of the camera with and without lens for the modified sound-guide with 1.5 mm diameter hole.

6.1.5 PCB Outside the Camera Housing

Figure 6.12 shows the measured results of the PCB with the original 0.5 mm diameter hole and the drilled 1 mm diameter hole with microphone and are situated outside the camera housing as seen in Setup 5 in figure 6.2 but without the sound-guide attached. The original PCB hole of 0.5 mm diameter shows a resonance frequency at 9500 Hz with an amplitude of 10.22 dB while the drilled PCB with 1 mm diameter hole shows a resonance frequency at 15820 Hz with an amplitude of 16 dB.

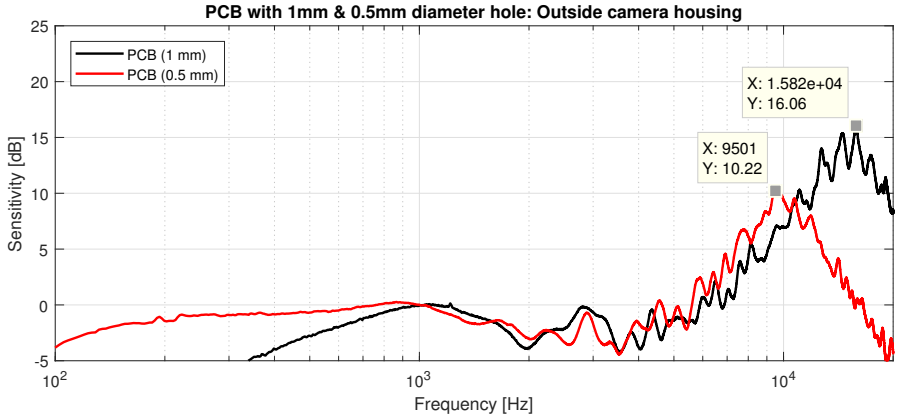

Figure 6.12: This plot compares the Frequency responses of the microphone with two different diameters of the PCB hole.

For the 1 mm PCB hole there occurs a attenuation at the low frequency range. This roll-of is similar to that of the MEMS microphone.

6.1.6 Sound-guide

The following measurements are taken by placing the acoustic path outside the camera housing with a porous material, which is 4.3 cm thick in between as shown by Setup 5 in figure 6.2. Figure 6.13 below shows the comparison of the three hole diameters used for the measurements. The original sound-guide (0.6/0.8 mm) gives rise to a resonance frequency at around 7300 Hz with an amplitude of 13 dB, the 1 mm sound-guide hole gives rise to a resonance at around 8000 Hz with an amplitude of 14.8 dB and the 1.5 mm sound-guide hole has an resonance at around 8500 Hz with an amplitude of 15 dB.

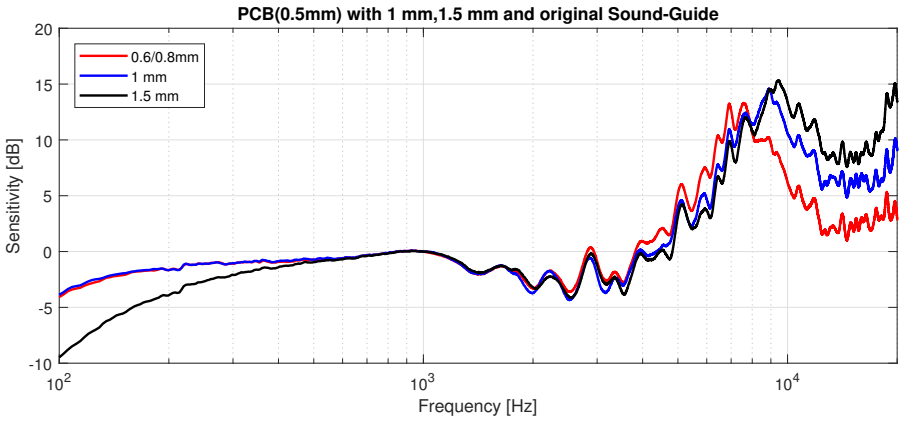

Figure 6.13: This plot compares the Frequency responses of the sound-guide with three different diameter holes, with the 0.5 mm diameter hole in the PCB

Figure 6.14 below shows the resonance of the three different hole diameters of the sound-guide when the hole in the PCB is 1 mm. For the original hole the resonance frequency occurs at 8140 Hz with an amplitude of 18.13 dB. For the 1 mm sound-guide hole the resonance occurs at 11020 Hz with a amplitude of 20.75 dB. And for the sound-guide with 1.5 mm hole the resonance occurs at 12730 Hz with an amplitude of 21.65 dB.

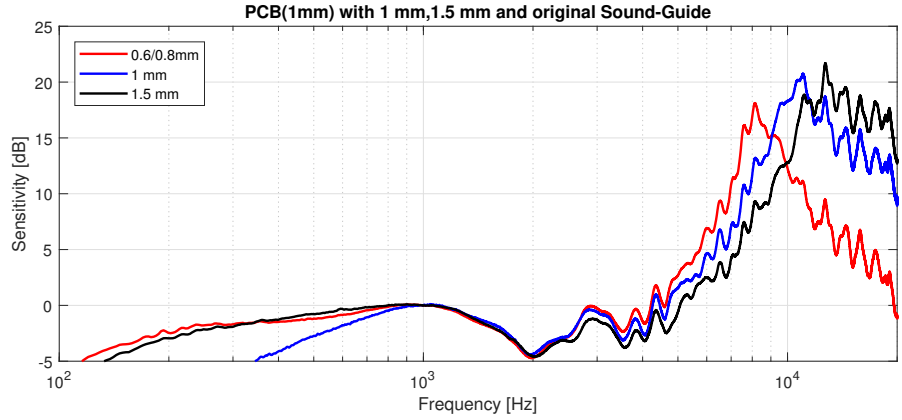

Figure 6.14: This plot compares the Frequency responses of the sound-guide with three different hole diameters, with the 1 mm diameter hole in the PCB.

6.1.7 Trimmed Sound-guide

In these measurements the sound-guide is trimmed in such way that only the part with the same length as the PCB remains (figure 5.3). The height of the trimmed sound-guide is 1.91 mm. The setup used is Setup 5 shown by figure 6.2. Figure 6.15 shows the results of the trimmed sound-guide with 1 mm and 1.5 mm hole with

the 0.5 mm hole in the PCB. For both the diameters it seems that the resonance frequency and amplitude is occurring at 9524 Hz with an amplitude of 13 dB.

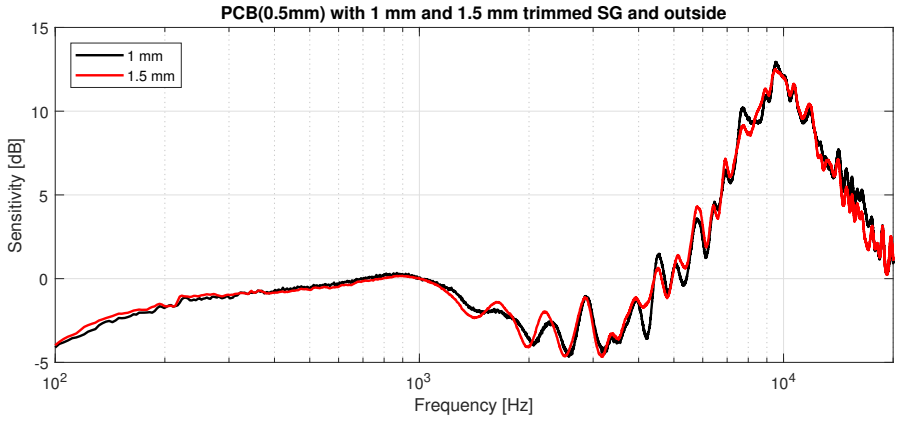

Figure 6.15: This plot compares the Frequency responses of the microphone with two different diameter on the trimmed sound-guide hole with the 0.5 mm hole in the PCB.

Figure 6.15 is shows the results of the trimmed sound-guide with 1 mm and 1.5 mm hole with the 1 mm hole in the PCB. For the sound-guide with 1 mm diameter hole the resonance frequency occurs at 12730 Hz with an amplitude of 18.2 dB and for the sound-guide with 1.5 mm hole the resonance frequency occurs at 14470 Hz with an amplitude of 14.88 dB.

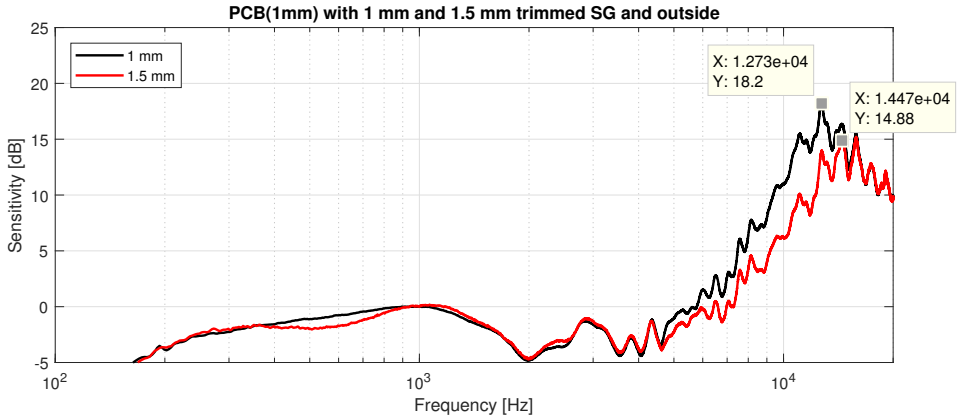

Figure 6.16: This plot compares the Frequency responses of the microphone with two different diameter on the trimmed sound-guide hole with the 1 mm hole in the PCB.

In table 6.1 below is the summarized results of all the measurement performed with the different diameters for the PCB and Sound-guide hole as well as for the trimmed Sound-guide.

Table 6.1: Table of the different measurements and their configurations of the acoustic path

Measurement Nr.	**PCB hole diameter** [mm]	**Sound-Guide Hole Diameter** [mm]	**Sound-Guide Hole length** [mm]	**Resonance Frequency** [Hz]
(1)	0.5	N/A	N/A	9507
(2)	0.5	0.6/0.8	3.81	7192
(3)	0.5	1	3.81	8903
(4)	0.5	1.5	3.81	9442
(5)	0.5	1	1.91	9519
(6)	0.5	1.5	1.91	9519
(7)	1	N/A	N/A	15820
(8)	1	0.6/0.8	3.81	8130
(9)	1	1	3.81	11020
(10)	1	1.5	3.81	12730
(11)	1	1	1.91	12730
(12)	1	1.5	1.91	14470

6.2 Simulation Results

6.2.1 Finite Element Method

In figure 6.17 below show the simulated results of the sound-guide with different holes, original, 1 mm and 1.5 mm hole. For the original hole the resonance occurs at 6492 Hz with an amplitude of 15.6 dB. For the 1 mm hole the resonance occurs 7518 Hz with an amplitude of 15.9 dB and for the 1.5 mm the resonance occurs at 8090 Hz with and amplitude of 16 dB.

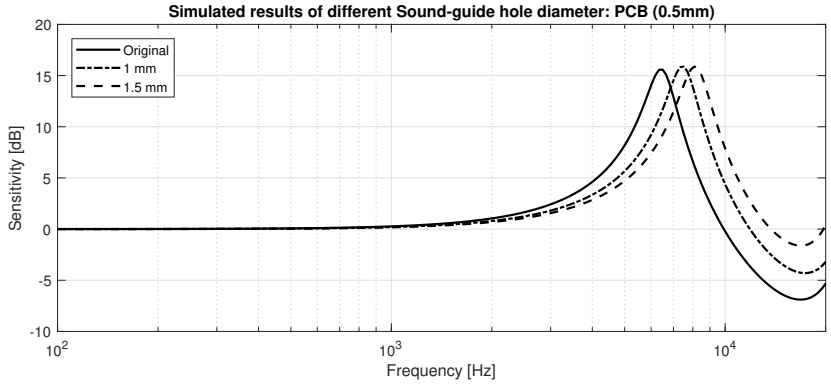

Figure 6.17: This plot compares the simulated frequency responses of the three different holes in the sound-guide, and the 0.5 mm hole in the PCB

Figure 6.18 below shows the simulated results of the sound-guide with different holes, original, 1 mm and 1.5 mm hole. For the original hole the resonance occurs at 6652 Hz with an amplitude of 16.46 dB. For the 1 mm hole the resonance occurs 8090 Hz with an amplitude of 16.9 dB and for the 1.5 mm the resonance occurs at 9143 Hz with and amplitude of 16.75 dB.

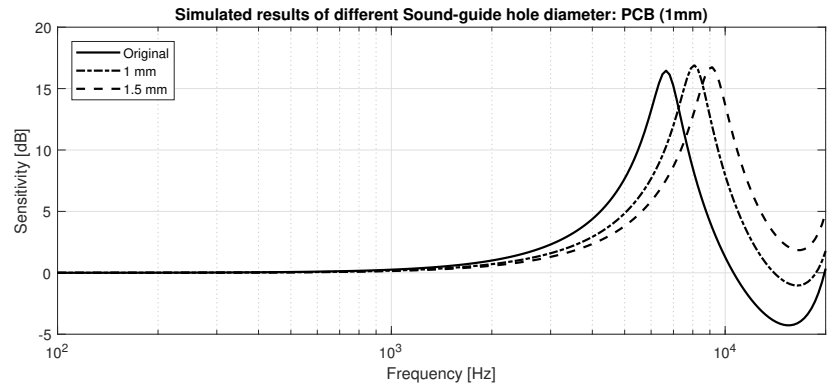

Figure 6.18: This plot compares the simulated frequency responses of the three different holes in the sound-guide, and the 1 mm hole in the PCB

The following simulations show the results of the trimmed sound-guide with 1 mm and 1.5 mm diameter holes. In figure 6.19 the top plot shows the simulation results when using the original 0.5 mm hole in the PCB together with the trimmed sound-guide with 1 mm and 1.5 mm hole. For the 1 mm hole the resonance occurs at 8090 Hz with and amplitude of 14.67 dB and for the 1.5 mm hole the resonance occurs at 8496 Hz with an amplitude of 14.47.

For the bottom plot in figure 6.19 the simulation results for when the hole in the PCB is 1 mm and with the trimmed sound-guide with 1 mm and 1.5 mm hole are shown. The resonance for the 1 mm hole occurs at 9143 Hz with an amplitude of 14.67 dB and for the 1.5 mm the resonance occurs at 10082 Hz with an amplitude of 13.62 dB.

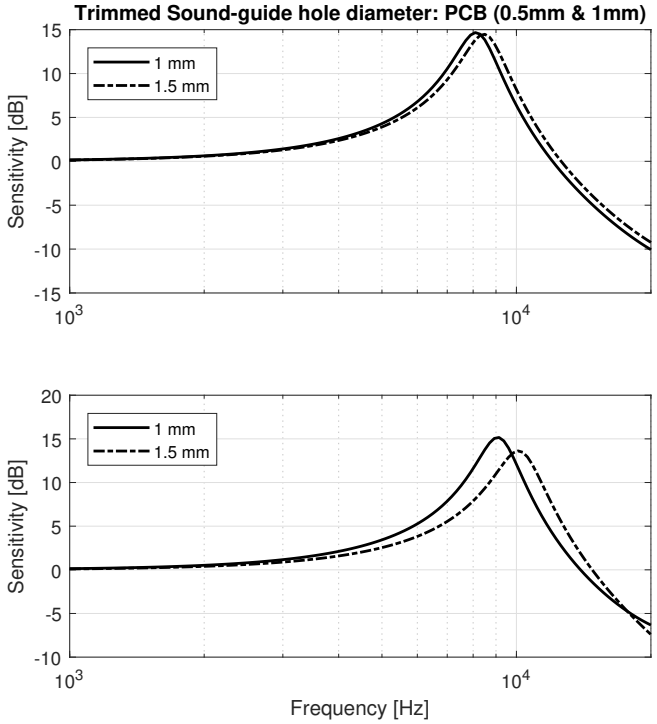

Figure 6.19: This plot compares the simulated frequency responses of the two different hole in the trimmed sound-guide with 1 mm and 0.5 mm hole in PCB

In table 6.2 below is the summarized results of all the simulations performed with the different diameters for the PCB and Sound-guide hole as well as for the trimmed Sound-guide. Simulation (1) and (7) show the simulation results of the different holes in the PCB without sound-guide

Table 6.2: Table of the different configurations of the Acoustic Sound Path

Simulation Nr.	**PCB hole diameter** [mm]	**Sound-Guide Hole Diameter** [mm]	**Sound-Guide Hole length** [mm]	**Resonance Frequency** [Hz]
(1)	0.5	N/A	N/A	8921
(2)	0.5	0.6/0.8	3.81	6492
(3)	0.5	1	3.81	7517
(4)	0.5	1.5	3.81	8090
(5)	0.5	1	1.91	8090
(6)	0.5	1.5	1.91	8496
(7)	1	N/A	N/A	10332
(8)	1	0.6/0.8	3.81	6652
(9)	1	1	3.81	8090
(10)	1	1.5	3.81	9143
(11)	1	1	1.91	9142
(12)	1	1.5	1.91	10082

Chapter 7

Analysis and Discussion

7.1 Comparison of Measured and Simulated results

Table 6.1 and 6.2 shows the measured and simulated results respectively of the different configurations of the acoustic path. Results (1)-(6) in both tables show the results when keeping the PCB hole constant at 0.5 mm diameter. For results (1)-(6) the difference between the measured and the simulated are not large, the smallest differences is about 500 Hz for measured/simulated number (1) while the largest difference is approximately 1500 Hz for measured/simulated number (5).
For results (7)-(12) when the PCB hole is enlarged by drilling the deviations become much larger. The smallest difference is about 1500 Hz for measured/simulated number (8) and the largest difference is about 5500 Hz for measured/simulated number (7). Comparing figure 6.13 and 6.18 the overall behavior can be observed. The comparison shows that the behavior of the frequency response is captured to a certain degree, with the exceptions that a lift of the high frequencies after the resonance occurs in the measured results and the attenuation which occurs only for measurement number (4) and for (7) and (9) for low frequencies, the reason for this attenuation is unknown. This low frequency attenuation is a characteristic retained from the MEMS microphone shown in figure 3.4 and only occurs for the measurements listed in the previous sentences.

These differences can be caused by several factors such as,

- Imperfect drilling in the PCB. The MEMS sound inlet is off-center from the PCB hole.
- Drilling may have cause small particles from the PCB to enter the MEMS sensor cavity causing disturbances of damaging the MEMS membrane.
- The soldering ring around the sound inlet of the MEMS microphone forms a small cavity when attached to the PCB.
- The gap created by the adhesive tape is not modeled.
- For the original real sound guide there is a fillet around the inlet and exit hole which is not modeled.
- The measurement setup was not sufficient when measuring the Acoustic system outside the camera housing as seen in Figure and shown by Setup 5.

The main reason is most likely the implementation of the fictive cavity. The real cavity caused a resonance around 40 kHz. The manufactures won't share the details of the design for secrecy reasons. One speculation could be that the front-chamber is connected to the back-chamber thus increasing the volume of the Helmholtz resonance cavity and producing a lower resonance. This was not observed when removing the package lid of the MEMS microphone and observing it under a microscope.

7.2 Effects on the Frequency Response by the Surrounding Components

The effects on the frequency response by the camera lens and camera face can be observed. In figure 6.9 and figure 6.10 shows the comparison between the camera with lens and without with two different hole diameters. For both these plots the same behavior occurs when the lens is removed, a slight attenuation occurring before and after the resonance peak, due to the reflected waves from the lens causing interference at these frequencies. This behavior is not present for the 1.5 mm hole in the sound-guide shown in figure 6.11.
The camera face is amplifying the frequencies with the same wavelength as the camera face dimensions. This effect can be seen in figure 6.8, where around 2.5 kHz a gain is seen, the wavelength of the lower frequencies is to large to hit the camera face, but when the wavelength is equal or smaller compared to the camera face those frequencies are amplified because of pressure doubling.
This is what could be causing the amplification after the resonance peaks for the measurements performed with Setup 5, where the Acoustic path with the MEMS microphone are located outside the camera housing. The length of the sound-guide is approximately 2 cm, which means frequencies around 17.5 kHz are amplified. Another suspicion for this lift of the higher frequencies could be the self-noise of the MEMS microphone.

7.3 Thermoviscous Losses

Figure 6.6 shows the consequences when waves propagate through narrow regions where the viscous and thermal boundary layers are formed, thus causing losses. The effect of these losses is most obvious for the resonance frequency. The resonance frequency shifts down in frequency and broadens the peak i.e. decreases the Q-value.
The individual effects of thermal conduction and viscous shearing are known. Viscous losses affects the sound pressure distribution while thermal conduction affects the resonance peak[12].

7.4 Different Geometries of the Helmholtz Cavity

To justify the simplification of using a cylindrical cavity instead of the real cavity geometry used in the INMP522 MEMS microphone, three different cavities were investigated. The simulation is performed in Pressure Acoustics where sound hard wall boundaries are used and without the application of thermoviscous losses. The simulation results show that the difference between the real and the cylindrical cavity are not large. Thus, the cylindrical cavity can be used, and the axis-symmetric model can be made to save computational time.
One thing to consider is that it is not know if thermoviscous effects were to be applied if the resonance peaks would still have the same difference or not. It is not known how the different geometries of the Helmholtz cavity coupled with thermoviscous will affect the resonance frequencies.

Chapter 8

Conclusions and Future Work

The phenomena that occurs during the capture of audio are identified and implemented in the FEM software. A computationally effective way was used to model the simplified system of the acoustic path, by simplifying the original geometry of the front chamber, an axis symmetric model could be used.

The acoustical path was investigated to find the best configuration to obtain a desirable frequency response. It was found that using a short, wide and uniform hole in the sound-guide coupled with a wide hole in the PCB but no wider than the sound-guide hole resulted in a resonance to occur in the high frequency range.

In certain applications amplifying the high frequencies is desirable because higher frequencies attenuated easier by impeding objects. It is also desirable that only the first half of the resonance occurs in the audible frequency range, because that way filter are more effective. The impact of the lens is insignificant while the camera face boost the frequencies that are in the same dimensions as the face. Thermoviscous losses are present when sound waves propagate in narrow region, to obtain simulated results that match the measured results these losses need to be included. This work is relevant for any electronic device using a MEMS microphone and serves as a guide to obtain the desired frequency response.

Although the simulated results did not match the measured results in terms of amplitude and resonance frequency the overall behavior of the sensitivity was captured. For future work the following points would require more work

- A more accurate model in 3D space dimension of the MEMS microphone should be modeled for a better match of the measured results.
- The materials used for the MEMS microphone should be known to obtain the correct resonance amplitude.
- This work could extend to other cameras using wave-guides of similar type. Simplified models could be made at first, and if needed more complexity could be added over time.

References

[1] "MEMS microphone INMP522 Datasheet | TDK." `https://www.invensense.com/products/digital/inmp522/`.

[2] M. Herring Jensen, "Theory of Thermoviscous Acoustics: Thermal and Viscous Losses," Feb. 2014.

[3] D. T. Blackstock, *Fundamentals of physical acoustics.* John Wiley & Sons, 2000.

[4] L. E. Kinsler, *Fundamentals of acoustics, 4th Edition.* Wiley, 2000.

[5] B. Hökmark, *Acoustic Analysis of Loudspeakers Cavity Including Viscothermal Effects.* Master's Dissertation, LTH, 2007.

[6] L. Li, Y. Liu, F. Zhang, and Z. Sun, "Several explanations on the theoretical formula of helmholtz resonator," vol. 114, 08 2017.

[7] A. K. Gupta and N. Gupta, "Development of Shape of Helmholtz Resonator Cavity for Attenuation of Low Frequency Noise of Pure Reactive Muffler," vol. 1, no. 6, p. 6, 2016.

[8] *Acoustics Module User's Guide.* COMSOL Multiphysics© v. 5.3a.

[9] ST.*com*, "AN4426: Tutorial for MEMS microphones," tech. rep.

[10] J. Widder and A. Morcelli, "Basic principles of MEMS microphones," Apr. 2014.

[11] "InvenSense, Microphone Specifications Explained." `https://www.invensense.com/download-pdf/an-1112-microphone-specifications-explained/`.

[12] D. Homentcovschi, R. Miles, P. Loeppert, and A. J Zuckerwar, "A microacoustic analysis including viscosity and thermal conductivity to model the effect of the protective cap on the acoustic response of a MEMS microphone," *Microsystem technologies : sensors, actuators, systems integration*, vol. 20, pp. 265–272, 2014.

[13] ST.*com*, "AN4427: Gasket design for optimal acoustic performance in MEMS microphones," tech. rep.

[14] S. Fei, *Development of a General Acoustics Model for an Arbitrary Camera Design.* Master's Thesis, BTH, 2018.

[15] M. Herring Jensen, "How to Model Thermoviscous Acoustics in COMSOL Multiphysics."
`https://www.comsol.com/blogs/`.

Faculty of Engineering, Blekinge Institute of Technology, 371 79 Karlskrona, Sweden